Diffuse Reflectance Spectroscopy for the Evaluation of Mid-Palatal Suture Maturation After Expansion

binhuan yuan
Marquette University

DIFFUSE REFLECTANCE SPECTROSCOPY FOR THE EVALUATION OF MID-PALATAL SUTURE MATURATION AFTER EXPANSION

by

Binhuan Yuan

A Thesis Submitted to the Faculty of the Graduate School,

Marquette University,

in Partial Fulfillment of the Requirements for

the Degree of Master of Science

Milwaukee, Wisconsin

May 2021

ABSTRACT
DIFFUSE REFLECTANCE SPECTROSCOPY FOR THE EVALUATION OF MID-PALATAL SUTURE MATURATION AFTER EXPANSION

Binhuan Yuan

Marquette University, 2021

Diffuse reflectance spectroscopy (DRS) is a technique for characterizing the optical properties of biological tissues and has been extensively studied for diagnosis and therapeutic monitoring of various diseases. This thesis investigates the potential use of DRS for the evaluation of mid-palatal suture maturation after expansion. The most common evaluation technique for palatal expansion is Computed Tomography (CT). The major issue with CT is that during serial radiological scanning, patients are repeatedly exposed to ionizing radiation. DRS is a non-invasive, non-ionizing method which can be used to quantify the tissue optical properties in the visible wavelength *in vivo*. This study demonstrates that a fiber-optic-based DRS system could be used to quantify the total hemoglobin content and scattering coefficient in the simulated dental tissue, showing its potential to be used to represent the maturation of mid-palatal suture.

ACKNOWLEDGEMENTS

Binhuan Yuan

Firstly, I would like to thank my advisor, Dr. Bing Yu for giving me the opportunity to work on this research project. Thank you for all your guidance, feedback, and patience with me in learning new knowledge and skills.

I would also like to thank Dr. Dawei Liu for introducing me to the dental field and evaluating palatal expansion maturation. All your support and help are highly appreciated.

Lastly, I would like to thank my parents, for their tremendous amount of support throughout my entire education. I would not have gotten this far without your encouragement, constant support, and trust.

Table of Contents

Chapter 1 INTRODUCTION

Rapid Palatal Expansion (RPE) is a conventional orthodontic treatment to correct dental malocclusion such as posterior crossbite and dental crowding. The overall goal of RPE is to expand the maxilla by separating the mid-palatal suture and other circummaxillary-sutures. Oral radiographs and computed tomography (CT) are the most used methods to examine the palatal expansion, but both methods use harmful X-rays. Among them, CT exposes patients to high dose ionizing radiation. A large proportion of patients receiving RPE treatment are teenagers, and the ionizing radiation from these measurements may cause long-term harms to these young patients.

Diffuse Reflectance Spectroscopy (DRS) is a non-invasive technique widely used in therapeutic and diagnostic applications in the biomedical field. DRS system has the potential to replace oral radiographs and CT technology for detection of mid-palatal suture maturation. In the process of RPE, blood gradually accumulates in the suture gap. During the ossification of mid-palatal suture after RPE, a large number of islands shape acellular tissue and inconsistent calcified tissue will be generated in the sutural gap. Changes in the blood content and bone density, and thus the maturation of the mid-palatal suture can be quantified by measuring the optical parameters using DRS.

The main objective of this research is to investigate the potential of using DRS as a non-invasive and cost-effective tool to evaluate the palatal suture maturation after RPE. In this study, a physical model was designed to simulate mid-palatal suture after

expansion, and the optical parameters of the model were measured using a fiber optic DRS probe.

In Chapter 2 introduces the history of RPE, and the current methods to assess mid-palatal suture maturation as well as their pros and cons. The phenomenon of blood enrichment and growth of new bones after RPE, which lead to the possibility of using DRS to assess mid-palatal suture maturation, are also included in Chapter 2. Chapter 3 describes the principle of DRS, related mathematical models to simulate light-tissue interaction, and its applications in characterization of biological tissues. In Chapter 4, a physical model of the RPE process of human maxilla is introduced and experiments are conducted to demonstrate that DRS has the potential to evaluate mid-palatal suture maturation. Major limitations of the current study are discussed and directions for future studies are proposed in Chapter 5.

Chapter 2 RAPID PALATAL EXPANSION

2.1 Mid-Palatal Suture

The palate is the roof of the mouth in humans and other mammals. It separates the oral cavity from the nasal cavity. The mid-palatal suture is a potential fissure in the middle of the palate, which is connected with connective tissue without complete osseous union. The mid-palatal suture is not a regular dividing line, but the left and right maxillary processes extend to each other interdigitated, forming an irregular line of mutual chimerism. During expansion, the potential cracks gradually expand, the number of blood vessels in the connective tissue increases, the blood supply becomes more abundant, and the number of fibroblasts increases.

2.2 The Background of Rapid Palatal Expansion

Rapid Palatal Expansion (RPE), as an orthodontic treatment, is commonly used in the correction of posterior crossbite and maxillary narrowness [1]. Normal occlusion means that the teeth of the upper jaw occlude with their opponents on the lower jaw. When the mandible is closed, the upper posterior teeth or molars are inwards of the lower molars, which is often called posterior crossbite. New South Wales Government defines the term overjet as a horizontal distance between the upper and lower front teeth. Large overjet describes a condition where the horizontal separation is greater than 2 millimeters. The skeletal or dental structure may cause maxillary transverse deficiency. RPE is a commonly used non-surgical maxillary expansion technique [2]. Expanding the dental arch's width can correct the maxillary width deficiency and posterior crossbite [3]. In recent years, orthodontics focuses more on smile aesthetics, emphasizing the

transverse dimension of the dental arch and minimizing the buccal corridor's visibility [1,4]. Many patients presented with dentofacial deformation or cleft lip and palate with restricted maxillary segments [5]. These patients have become potential therapeutic users of RPE.

Dr. Emerson C. Angell first reported the use of RPE in orthodontics in 1860. Many practitioners tried and improved RPE from different views in the early stage [49]. Over a century after the first RPE publication, Hass demonstrated that RPE is effective in the treatment of maxillary or nasal insufficiency through successful animal experiments and subsequent human trials [3].

In the current orthodontic treatment of palatal expansion, there are many different methods for doctors and patients to choose which include tooth-borne expanders, bone-borne maxillary expansion devices, and surgically assisted rapid palatal expansion (SARPE) [1,5,6,7]. Selection of treatment options depends on many treatment limitations.

For patients with transverse discrepancy, the earlier intervention can achieve a better treatment effect, especially if the treatment time is set before the peak skeletal growth [8]. However, there are significant differences in skeletal maturation among individuals, and there is no obvious correlation with age and gender [7]. In the actual orthodontic process, how to accurately determine the maturation of palatal suture has become a very important part of the treatment, which by far is largely relying on the clinical experience of orthodontists. If the RPE is misdiagnosed to be complete, an ideal expansion treatment cannot be maintained, leading to unstable results and relapse [8]. The main side effects of RPE included but not limited to acute pain, gingival recession,

dehiscence formation, palatal mucosa necrosis, buccal dentoalveolar tipping and poor long-term expansion stability [7,8].

According to the structure and degree of maxillary suture fusion, different techniques, such as invasive biopsy, CT, have been put forward to assess suture maturation. Among them, biopsy is invasive and thus causes a certain degree of trauma and pain to patients. CT can achieve excellent detection efficiency, but patients are exposed to harmful radiation which limits its use in evaluating the structure and degree of maxillary suture fusion. In particular, because most of the patients receiving RPE are teenagers, the use of CT may have long-term harmful impact on these young patients.

2.3 Current Methods to Assess Mid-Palatal Suture Maturation

2.3.1 Animal and Human Histologic Studies

In the early experimental studies, scientists investigated the postnatal development of the hard palate in adolescents and fusion of palatal suture after surgical treatment through histologic studies of humans and animals. Most of these studies used conventional histologic and micro-radiographic methods on autopsy materials [10, 11]. Melsen B., et al. indicated that, through the analysis of histologic autopsy, the growth of hard palate length continued to 13 to 15 years old, and the shape of transverse suture changed during postnatal development [10]. Persson M. showed that mechanical force during bone growth alters the remodeling of sutured joints, but with advancing age, the sutures are covered with calcified tissue and synovium [11]. By understanding the differences of mid-palatal suture in different individuals and the possible expansion fusion situation of adolescent patients prior to surgery, a dentist can effectively achieve orthodontic treatment without invasive surgical assistance.

Histologic studies can effectively avoid the difficulty in judging the degree of palatal suture fusion *in vivo* and provide a standard reference for evaluating expansion maturation in orthodontic diagnosis and treatment. However, such implementation requires obtaining biopsy samples from the patient and continuous occlusal radiology also causes image overlap [7], leading to inaccurate diagnosis.

2.3.2 Computed tomography

CT is a widely used clinical imaging technique. It uses accurately collimated X-ray beams, gamma rays, and high-sensitivity detectors to make cross-sectional scanning around a part of the human body, and finally get the internal structure image of the target. Because of its strong penetrability, CT can easily detect changes of maxilla bone after RPE treatment. Franchi L., et al. evaluated the bone formation of the mid-palatal suture in 17 patients before rapid maximal expansion (T0), after active expansion (T1), and six months after convalescence (T3), and compared the images at different periods [12]. All subjects were aged from 8 to 14 years old, and with malocclusions such as maxillary arch stenosis or unilateral or bilateral posterior crossbite.

After RPE, the healing of mid-palatal suture can be predicted by a variety of morphological parameters, including obliteration index, outcome length, linear vertical distance, and bone density in the sagittal plane [13]. In a low-dose CT study, multi-slice CT scans were taken at T0, T1 and T2. The images were used to calculate the density values and the Mann-Whitney U test was used to compare the density between sutural region of interests (ROIs) and the bony ROIs. It was found that RPE successfully opened the palatal suture [12].

Although CT technology can intuitively detect and evaluate the maturation of mid-palatal suture, it has several limitations. During serial radiological scans, patients are exposed to radiation multiple times, which can cause irreversible damage to tissue or organs. A considerable number of patients treated with RPE are adolescents, and the effect of radiation on brain development should be seriously considered.

2.3.3 Ultrasonography (USG)

Medical ultrasound is also widely used for imaging internal body structures, such as joints and blood vessels. Ultrasonography transmits ultrasonic signal pulses to biological tissue through an ultrasound probe, detects the echo of signal pulses, and utilizes the different reflection characteristics of the tissue to form images. Maffulli N., et al. have shown that USG can be used to evaluate dispersion osteogenesis wounds in long bones with high stability and test precision [14]. Compared to CT, ultrasonography can achieve real-time image generation and does not require patients to be repeatedly exposed to high dose ionizing radiation, and thus is safer. However, the ultrasonography images are relatively fuzzy and are not easy to distinguish the fusion of mid-palatal suture. USG is mainly for subjective visual inspection and there is no quantitative measurement information for the time being [9].

2.4 Physiological and morphological changes after rapid palatal expansion

The main function of RPE is to increase the upper arch transverse dimensions. The increase of mid-palatal suture separation with force is accompanied by an influx of blood, which is then followed by new bone formation. During the ossification of mid-palatal suture, a large number of islands-shape acellular tissue and inconsistent calcified tissue are generated in the middle of the sutural gap, and bone spicules are generated at

the suture margins. The generation of bone spicules and tissue is random, and the overall distribution is uneven. With the increase of the number of bone spicules, some areas are separated by connective tissues, and the content of enriched blood decreases, resulting in the formation of woven bone [45].

Alberto C., et al. [56] aimed to investigate immediate histologic changes in mid-palatal suture after RPE and collected the biopsy samples at 7 and 30 days after RPE. In the 7-days samples, histomorphometry showed that there were 14% newly formed bone in the mid-palatal suture, and the rest included soft tissue and blood clot (caused by the trauma of maxillary expansion). Newly formed trabeculae were surrounded by osteoid matrix and grew in parallel. Within the suture, several blood clots and large blood vessels were observed. In the 30-days samples, histomorphometry showed 43% newly formed bone and 57% soft tissue and small blood vessels. The reported case showed that within the expansion of mid-palatal suture, the total blood volume in the suture region increased in the early stage. During bone growth, the total blood volume decreased.

Chapter 3 DIFFUSE REFLECTANCE SPECTROSCOPY

3.1 Background

In recent years, optical methods are playing an increasingly important role in the diagnosis and treatment of various diseases. In particular, diffuse reflectance spectroscopy (DRS) has been extensively studied in many organ sites, such as breast, esophagus, bronchus, brain, pancreas, GI tract, and cervix to characterize pre-cancers and cancers [15-24]. The working principle of DRS is to illuminate the surface of a biological tissue or other turbid medium with broadband light, mostly through an optical fibers or fiber bundle, and the photons diffusely propagate in the tissue experiencing multiple scattering and absorption events. Photons re-emitted from the same surface, called diffuse reflectance, are collected by a detection fiber or fiber bundle, and converted to a spectrum in a spectrometer. The intensity of the reflectance spectrum depends on the light scattering and absorption properties of the tissue sample [25]. By analyzing the diffuse reflectance spectrum, the tissue optical properties, such as absorption coefficient ($\mu a(\lambda)$) and reduced scattering coefficient ($\mu s'(\lambda)$) can be accurately extracted. Tissue scattering is caused by local reflection index mismatch in biological tissues and mainly determined by the size, density, and refractive index of particles (called scattering centers). For example, the difference between the reflection index of cytoplasm and organelles, such as cell membrane, nuclei, mitochondria, etc., results in change of light transmission direction [46]. In the visible spectrum, hemoglobin is the dominant light absorber. The absorption spectrum of oxy- and deoxyhemoglobin are different, thus analysis of the absorption spectrum of biological tissue, using Beer-Lambert Law of light absorption,

can be used to determine the hemoglobin concentrations and blood oxygen saturation (SO_2) [26].

3.2 Mathematical Models for Light Tissue Interaction

Light can pass through the surface of biological tissue and interact with tissue components, thus generating light reflection and transmission. The design and application of bio-photonic devices heavily rely on analytical mathematical or numerical models to simulate light propagation in turbid biological tissue and to characterize its optical properties. Mathematical models commonly used in DRS system are discussed below.

3.2.1 Light-tissue interaction

The propagation of light in biological tissue depends on the optical characteristics of the tissue and light wavelength. Interaction of light with tissue leads to light attenuation due to absorption and scattering. After the light is absorbed in biological tissues, the molecule that absorbs photon energy changes from the ground state to the excited state. The absorbed energy can trigger some chemical reactions, or a portion of the absorbed energy can be re-emitted as light. Hemoglobin, oxy-hemoglobin, beta-carotene, melanin, and bilirubin are the absorbers of visible radiation. The primary absorber in biological tissues is hemoglobin [50].

Light interaction with a turbid medium, such as biological tissue, through scattering can result in change of the direction of light propagation. In general, the wavelength of light does not change during a scattering process (except for Raman scattering). Light scattering is dependent on the scatter size and distribution, incident wavelength, and refractive index of the scatterer [47]. When the size of the scatterer is much smaller than the wavelength of light, Rayleigh scattering dominates and is often

used to calculate scattering coefficient. When the size of the scatterer is close to or larger than the wavelength of the light, Mie theory is used to calculate the scattering coefficient. Dominant scatters in tissue are relatively large in size, such as cell membrane, nuclei, collagen fibers, and mitochondria. In Mie scattering, visible light is scattered more in the direction of propagation (i.e., forward scattering) than in any other direction. Mie scattering is best suited for simulating the scattering in the visible light band of 430-630nm.

3.2.2 Monte Carlo Forward model

The propagation of light in biological tissue depends on the microstructure and physiological properties of tissue. The transportation equation of light in biological tissues (turbid media) can be described by Boltzmann equation [51], Eq. 1.

$$\hat{s}.\nabla L(\vec{r},\hat{s}) + \mu_t(\vec{r})L(\vec{r},\hat{s}) = \mu_s \int_{4\pi} p(\hat{s},\hat{s}')L(\vec{r},\hat{s}')dw' + S(\vec{r},\hat{s}') \quad (1)$$

Where, L is the radiance at location $\vec{r}$ within the tissue, μ_t is the total attenuation coefficient, $\mu_t = \mu_a + \mu_s$ (μ_a and μ_s are absorption coefficient and scattering coefficient, respectively), p is the phase function and S is the source term.

Diffusion theory (DT) is a fast and convenient analytical model of light transport. It is an approximate solution of the transport equation which yields the relationship between the optical properties and light fluence. The approximate validity of DT needs to ensure that the distance between the boundary of turbid medium and the light source is much larger than mean free path ($1/\mu_t$), and photons need to be scattered many times before being absorbed. Therefore, DT model cannot solve the boundary problem in layer

tissue, and DT model is also not applicable when the absorption is far stronger than scattering [51]. In such situations, a numerical model, the Monte Carlo model is often used to simulate the light propagation in turbid medium.

The Monte Carlo model is based on the theory that photons undergo a random trajectory in tissue, and the step size and direction of scattering can be determined by stochastic sampling of probability distributions [27]. In general Monte Carlo simulation, photons come in from the edge of biological tissue and randomly determine its initial direction and trajectory. It uses probability density function including scattering coefficient to obtain the traveling distance and optical path of photons in the medium. The weights of all photons entering the tissue is set to 1 and absorption by reduces the weight according to the Beer-Lambert law [48]. Monte Carlo model is numerical model, which is computationally extensive, and thus the full simulation is time consuming. Because tissue absorption and scattering coefficients are expected to change dynamically in tissue, the computationally extensive model limits the usability of Monte Carlo model for continuous monitoring of changes in $\mu_a(\lambda)$ and $\mu_s'(\lambda)$.

3.2.3 Monte Carlo Inversion model

Researchers have developed numerical and analytical models to extract scattering and absorption coefficients from a diffuse reflection spectrum. In this thesis, we use a flexible and fast Monte Carlo-based model of diffuse reflectance developed by Palmer et al. [33] to monitor the dynamic changes of scattering and absorption coefficients of turbid media. This model is based on a scaling approach which runs single Monte Carlo simulation for multiple photons. Many optical parameters can be obtained by this simulation. For a given photon with different absorption and scattering coefficient, the

corresponding optical parameters can be calculated by scaling relationship. It also created a look-up table method to make it suitable for real time detection. The model is suitable to fiber-optic-based measurements of diffuse reflectance spectra from infinite- or semi-infinite medium, and it uses a single reference measurement for calibration.

Palmer's model consists of two parts: a forward model to run Monte Carlo simulations and an inverse model to extract optical parameters of biological tissues. The absorption coefficient is mainly affected by the compositions in biological tissues and the scattering coefficient is related to the size and density of scattering structures in the tissue. In the forward model, the physiological and structural properties of the tissue are the inputs that are used to generate a diffuse reflectance spectrum. The concentration of each chromophore and the corresponding wavelength-dependent extinction coefficient are used to determine $\mu_a(\lambda)$, and Mie theory for spherical particles [31] is used to calculate the reduced scattering coefficient $\mu_s'(\lambda)$ and anisotropy factor (g). The optical properties $\mu_a(\lambda)$, $\mu_s'(\lambda)$ and g(λ) will be the inputs to establish a Monte Carlo model in the range of special wavelengths [32].

In the inverse model, the absorber concentrations, the scatterer size and density and the fixed free parameters will be initialized to use the Monte Carlo model of diffuse reflectance. The fixed parameters are the extinction coefficients of the absorber and the refractive index of the scatterer and the surrounding medium for a given wavelength. The reflectance spectrum modeled by the forward model is compared with the measured reflectance spectrum using a Gauss-Newton nonlinear least-squares algorithm to minimize the sum-squares error between the two spectra. To ensure that the convergence

reaches to the global minimum, the whole procedure will be iterated for each sample with a different, randomly chosen starting parameters. $\mu_a(\lambda)$, $\mu_s'(\lambda)$ and g(λ) are extracted from the model after the convergence [33].

3.3 Applications of DRS

DRS has a wide range of non-medical application scenarios, including color matching and identification in textiles, and characterizing and measuring mineral content in soils [34]. In the past two decades, DRS technology has been extensively studied for use in the medical field after continuous improvement, and it has made great progress in many research directions. Studies have shown that DRS has the ability to help improving surgery, chemotherapy, radiation, or a combination of above [52, 53]. It also has the potential of detecting bone cracks in the lengthen or even the palatal suture after the rapid palatal expansion [14]. Optical properties, such as absorption and scattering, can change dramatically with changes in biological tissue structure, vasculature, and metabolic function in the early and middle stage of cancer [35]. In recent years, DRS combined with an appropriate mathematical model has become more effective in quantification of physiological parameters of cancerous cells [36].

Chang et al. combined the DRS system with an inverse Monte Carlo model to characterize and compare the optical biomarkers between cervical intraepithelial neoplasia and normal cervical tissues [36]. It was found that total hemoglobin was a lot higher in high grade cervical intraepithelial neoplasia than normal cervical tissues. Langhout et al. combined fluorescence spectroscopy with the DRS system to characterize the difference of optical parameters between healthy and malignant colorectal tissues from surgery and calculated the difference in the concentrations of basic water, fat, and

hemoglobin [37]. DRS has also been employed for detection of diabetic foot ulcers, pressure ulcers, and reliable identification of tumor tissue in breast, lung, and liver [38-41].

3.4 Fiber-optic-based DRS

Fiber-optic-based DRS is a noninvasive technique that provides quantitative information such as absorption (μa(λ)) and reduced scattering (μs'(λ)) about tissue *in vivo*. It is a lightweight, portable, and robust device which uses a white LEDs as the source and a fiber optic spectrometer that converts light signal into a spectrum.

Yu et al. [42] fused visible of DRS to characterize normal tissues in the oral cavity. A pressure sensor was installed in the probe to monitor the contact pressure between the probe and cervix tissue during DRS measurement, so as to control and adjust the pressure to minimize its impact on the blood flow in tissues.

Vivek et al. [43] assembled a temperature sensor into the DRS system to monitor tissue temperature and optical properties during thermal coagulation of *in-vitro* tissues. The study found that reduced scattering coefficient of liver tissue decreased during heating due to tissue carbonization.

Hong et al. [54] developed a portable, lightweight, and low-cost DRS system using a smartphone-based spectrometer. This application was originally intended to measure the hemoglobin in epithelial tissue for economically underdeveloped areas where there is no infrastructure for routine diagnosis of epithelial cancer or precancer.

Chapter 4 MEASURING HEMOGLOBIN CONCENTRATION IN SIMULATED MID-PALATAL SUTURE

4.1 Introduction

Optical monitoring can be a portable and cost-effective alternative for monitoring mid-palatal suture maturation process. The purpose of this chapter is to demonstrate that DRS system has the potential to detect changes in hemoglobin concentration in the process of expansion in the healing period of mid-palatal suture. The RPE process of human maxilla is simulated by a physical model composed of bone, mucous membrane and blood enriched into the suture gap. This physical model is then used to study changes in the absorption coefficient and hemoglobin concentration of the physical model. Further, these changes are compared with the trend of blood content changes after RPE.

4.2 Materials and methods

4.2.1 DRS Instrument

The DRS system is shown in Fig. 4.1. It is consisted of a customized visible spectrometer (Avantes BV, The Netherland) with a white light-emitting diode (LED) as the light source, a laptop installed with custom software, and a customized fiber-optic probe. The fiber-optic probe consists of four fibers (200/220/240 μm) for illumination and one fiber (400/440/480 μm) for detection. The separation between each illumination fiber and the detection fiber is 2 mm, and the five fibers form a 90 degrees circular arc with the detection fiber as the circle center mounted into a 3D printing plate (4.1mm in radius), shown in Fig. 4.2. The illumination fibers are connected to the white LED to provide a stable light source and the detection fiber is connected to the spectrometer. A

customized LabVIEW program and MATLAB scripts for DRS system are installed in the laptop, which are used for instrument control, data acquisition and data analysis.

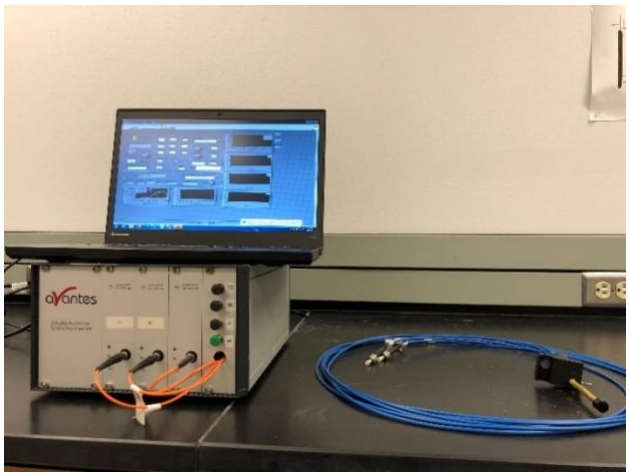

Figure 4.1: The fiber-optic DRS system with the fiber-optic probe

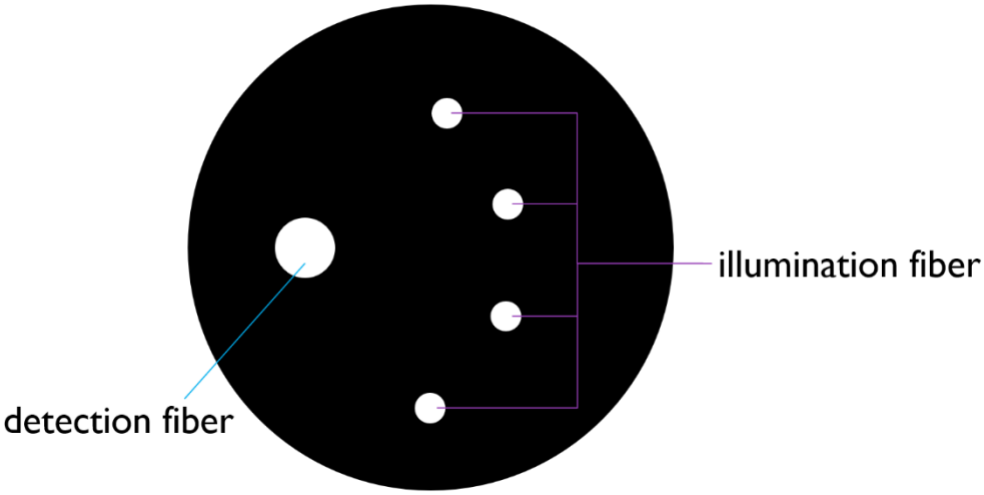

Figure 4.2: The geometry of the fiber-optic probe

4.2.2 Tissue phantom experiment

To evaluate the accuracy of the fiber-optic probe for measuring optical properties, 16 liquid phantoms were prepared to simulate the absorption and scattering properties of mid-palatal suture after RPE. These phantoms were composed of human hemoglobin (H0267, Sigma-Aldrich Co. LLC) as an absorber and polystyrene beads (07310-15, Polysciences Inc.) as a simulated tissue scatterer in aqueous solution. The mean absorption coefficient (wavelength range of 450-630 nm) $\mu_a(\lambda)$ for the phantoms ranged from 0.5 cm^{-1} to 4.3 cm^{-1} which was independently determined with a spectrophotometer (Lambda 35, PerkinElmer Inc.). The reduced scattering coefficient was calculated by Mie theory, the density and refractive index of the polystyrene beads. The reduced scattering coefficient $\mu_s'(\lambda)$ is lessened from 13 to 7 cm^{-1} due to the hemoglobin titration.

4.2.3 *In-vitro* experiment

In this study, a biophysical model was constructed to simulate changes of the mid-palatal suture after RPE. The small intestinal mucosa of pig was used as the mucosal structure covering blood and bone in the physical model in the experiment. The small intestinal mucosa was purchased fresh from a local grocery and stored at 4℃ to prevent water evaporation and mechanical damage. Human hemoglobin (H0267, sigma Aldrich Co. LLC) was used to prepare the solution to simulate the blood clot deposited in the gap after RPE, and the absorption coefficient of the solution was close to the normal blood [55] (The $\mu_a(\lambda)$ of the normal blood is 0.210±0.002 mm^{-1}) in the suture expansion. The purchased bone powder was stored at room temperature (22℃) and used to simulate the uneven growth pattern of bone after RPE.

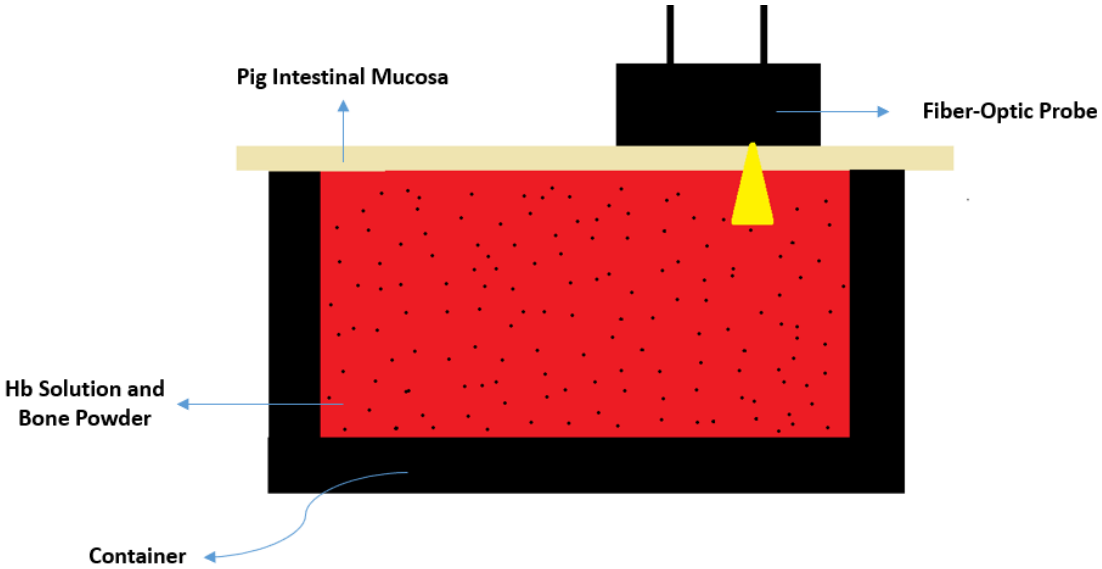

Figure 4.3: Experimental set-up to study the optical properties of a physical model simulating the mid-palatal suture after its response to expansion.

The cube shaped container, as shown in the Fig. 4.3, was made by 3D printing. There was a groove of (1x1x1cm) in the middle of the container, which was used to hold the mixture of bone powder and hemoglobin solution. The average thickness of mucous membrane was 1 mm. The mucous membrane was placed on the container and gently touched with mixture. In this experiment, five containers were fabricated and filled with different proportions of bone powder and hemoglobin solution to mimic the dynamic relationship between the silted blood and the new bone formation during an actual RPE process. Because bone powder particles are large and insoluble in water, the bone powder and hemoglobin solution might not be completely uniform. Therefore, five different locations on each sample were measured and averaged to minimize the effects of non-uniformity. To make a measurement, the fiber optic probe was placed perpendicular to

the mucosal plane. For each sample, 10 DRS measurements made from each of the five locations. For each measurement, the reflection spectrum, scattering coefficient, absorption coefficient, and hemoglobin concentration were recorded for further analysis.

Because the mean photon penetration depth within tissue is related to illumination detection separation and light wavelength, the mean penetration depth is far less than the depth of the groove. Therefore, the container has no effect on the measurement of diffuse reflection.

4.2.4 Data analysis

The absorption coefficient and reduced scattering coefficient of 16 phantoms were extracted by the Monte Carlo inverse model of reflectance. The spectrum of each phantom was used as a reference to invert other phantoms. The phantom that resulted in the smallest average error was selected as the reference phantom for inverting the diffuse reflectance spectra obtained in the tissue experiments. The extracted $\mu_a(\lambda)$ and $\mu_s'(\lambda)$ were averaged in the range of 450-630 nm. The absorption spectrum was used to calculate the hemoglobin concentration using the Beer's Law.

Student's t-test (significance level α=0.05) is a statistical technique to determine whether the means of two sets of data are significantly different from each other. The t-test was used to test whether the difference between the extracted hemoglobin concentration at different proportions of hemoglobin solution and bone powder were significantly different from each other.

4.3 Results

4.3.1 Phantom experiment

The raw spectrums of the phantoms are shown in Fig. 4.4. Comparing the spectra of different phantoms, it is found that human hemoglobin has two main absorption peaks at 540 nm and 570 nm wavelength. The absorption coefficient and the reduced scattering coefficient extracted from all phantoms are compared with the expected values, and the results are shown in Fig. 4.5 and Fig. 4.6, respectively. For $\mu_a(\lambda)$ and $\mu_s'(\lambda)$ extracted by all phantoms, the overall average error is 6.10% and 14.47%, respectively. The extracted $\mu_a(\lambda)$ has a smaller error and agrees better with expected value of the phantoms than $\mu_s'(\lambda)$. When the value of expected $\mu_s'(\lambda)$ exceeds 16, the deviation between extracted value and expected value increased. Therefore, it is necessary to avoid large $\mu_s'(\lambda)$ in the process of tissue experiment.

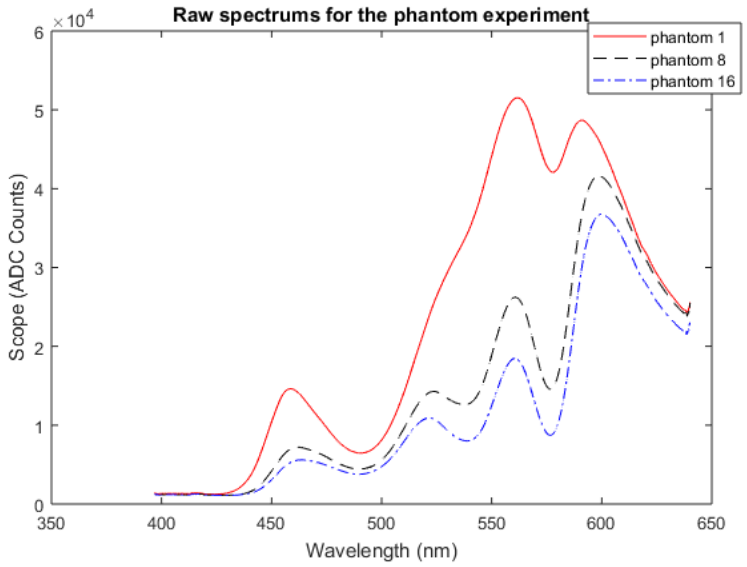

Figure 4.4: Raw spectra of the phantoms

The ninth phantom of the experiment (with overall errors for $\mu_a(\lambda)$ and $\mu_s'(\lambda)$ of 4.21% and 9.08%, respectively) was selected as a reference phantom for the DRS system to calibrate the Monte-Carlo model for tissue measurements.

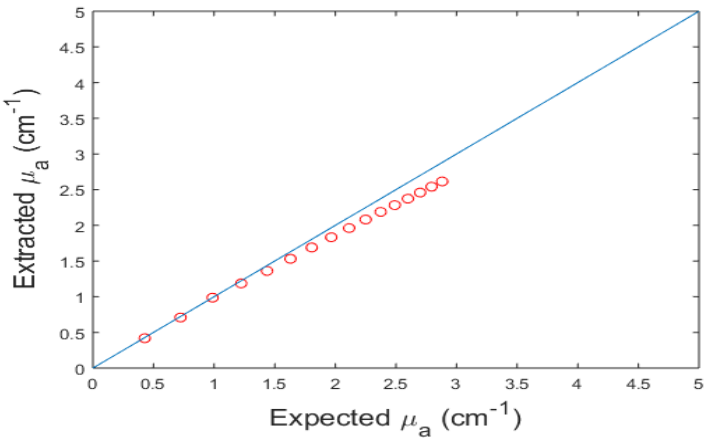

Figure 4.5: The extracted and expected $\mu_a(\lambda)$ of the phantom experiment

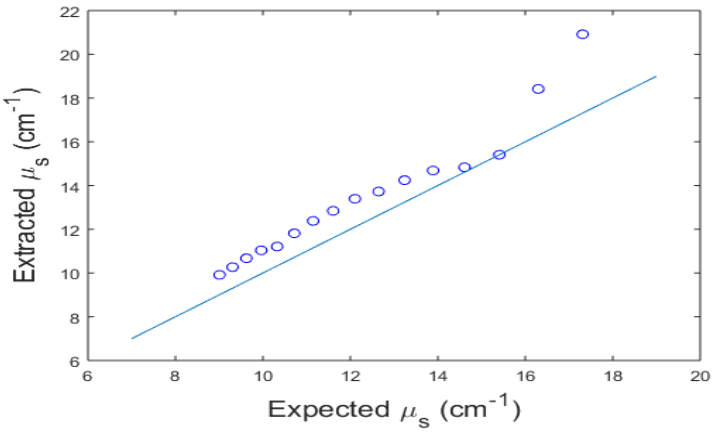

Figure 4.6: The extracted and expected $\mu_s'(\lambda)$ of the phantom experiment

4.3.2 *In-vitro* experiment

Five different containers were filled with different proportions of bone powder and hemoglobin solution and the expected concentrations are shown in Fig. 4.7. The concentration of stock hemoglobin solution was 41.15 µM/ml, different amounts of the

stock Hb solution were added to each container. In the first three containers, the content of hemoglobin solution gradually increased to simulate the process of RPE, representing the gradual expansion of the mid-palatal suture, which resulted in the formation of a cavity in the area detected by fiber optic probe as well as blood enrichment along with time. In the same process, because the bone is stretched to both sides, the bone content in the detection area gradually decreases, so in the first three containers, the corresponding content of bone powders were gradually decreased. The third container represents when the expansion reached the maximum state. The last two containers represent after the expander is reached to the maximum and fixed, and the bone slowly grow back over time. In the detection area of probe, the original enriched blood clot is replaced by newly grown bone. Therefore, the content of hemoglobin solution is expected to decrease, the content of bone powder increases correspondingly, and finally returns to the baseline.

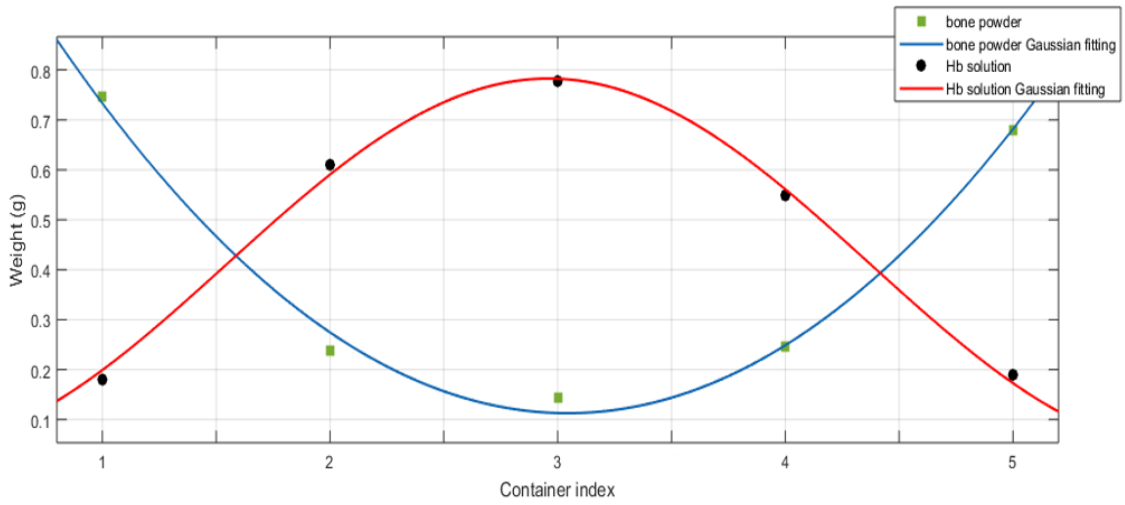

Figure 4.7: The trend of bone powder and Hb solution content

The measured hemoglobin concentration and average extracted $\mu_s'(\lambda)$ for the five containers were shown in Fig.4.8 and Fig.4.9, respectively. For visual comparison, the extracted hemoglobin concentration generally agreed with the expected values well, and both increased first and then decreased. The measured hemoglobin concentration for the baseline (1st container) was 9.91 μM/ml (central area detection). In the baseline, the measured hemoglobin concentrations of the five different detection points were 9.36±4.02 μM/ml, which shown a great difference compared to the results of the second container which were 24.95±5.65 μM/ml ($p = 0.014$). There are significant differences between the measurements of any adjacent containers, and they followed the trend of the expected hemoglobin contents. In order to simulate the RPE process, the first three containers (ascending process) and the last two containers (Descent process) changed in the order of adding hemoglobin or bone meal. In the ascending process, bone powder was added into the container first, and then hemoglobin solution was added afterward to simulate the process of blood flowing into the cavity after bone separation. In the descent process, the order of adding is opposite, simulating the process of bone growth and blood content decreasing. The proportions of hemoglobin and bone powders in containers 1 and 5 were the same, but the addition order was different, and the measured concentrations were 9.36±4.02 μM/ml and 10.74±4.54 μM/ml, respectively, which within the same range.

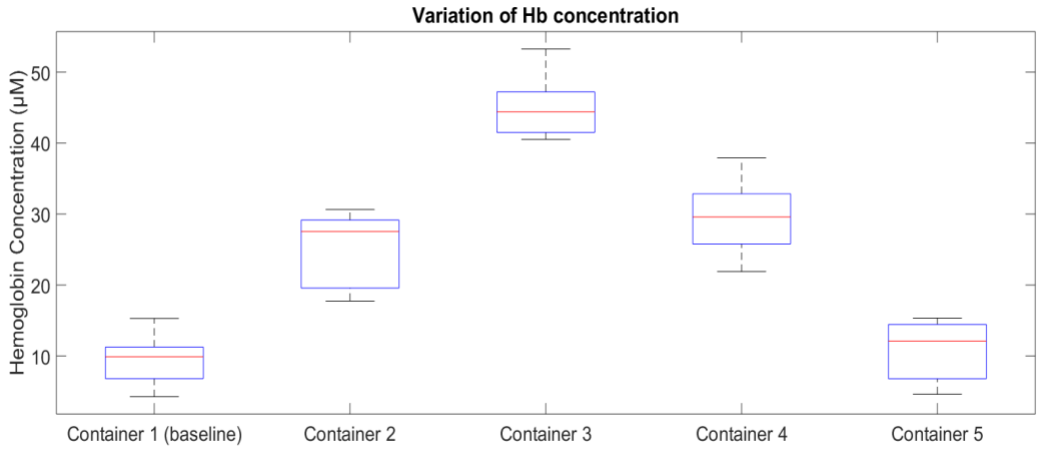

Figure 4.8: Measured Hemoglobin concentration for the five containers

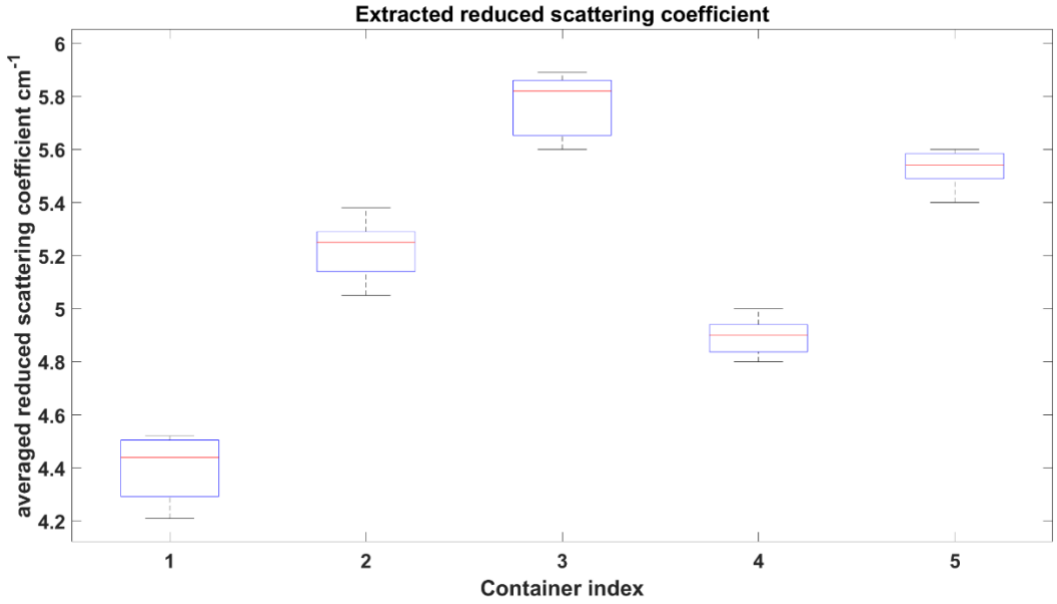

Figure 4.9: The extracted average $\mu_s'(\lambda)$ for the five containers

It should be noted that the bone powder used in this experiment is steamed bone powder made from animal bone. Compared with the characteristics of human bone, the contents of phosphorus and calcium in animal bones are higher, and the fat and protein contents are lower. Therefore, it is necessary to compare the optical properties between animal bone and bone powders. The absorption coefficient of animal bone and bone powders detected by the fiber-optic probe were both close to $0.1\ \mathrm{cm}^{-1}$. However, the extracted scattering coefficient of different detection positions of animal bone were quite different, varied between 12 and 14 cm^{-1}. In contrast, the extracted scattering coefficients of bone powders were around $8.1\ \mathrm{cm}^{-1}$ with little change. The extracted $\mu_s'(\lambda)$ for the first four containers followed the trend of the expected bone powder contents. Bone powders can affect the scattering coefficient, and they are insoluble in water, which makes the paste-like mixture effects scattering. Therefore, there might be an experimental error in the extracted scattering coefficients due to the proportion of mixture change during measurement.

4.4 Discussion

Noninvasive and quantitative assessment of the maturation of mid-palatal suture after RPE is of great clinical value to orthodontics and related surgical treatment. Computer tomography is an established technology that has been used to assess mid-palatal suture, but it can lead to unnecessary exposure to excessive radiation, causing damage to patients beyond surgical treatment. While DRS system cannot directly image the healing of mid-palatal suture, it can quantitatively analyze the hemoglobin contents and scattering coefficient of the mid-palatal suture without introducing radiation injury. In this study, a fiber-optic DRS system was modified to collect diffuse reflectance spectra

in the visible wavelength from simulated mid-palatal sutures that were obtained by mixing hemoglobin solution and bone powders at different proportion. The experiments showed reasonable $\mu_a(\lambda)$, $\mu_s'(\lambda)$ and hemoglobin values of the physical model quantitatively, which demonstrates that the DRS system has the potential to detect the maturation of mid-palatal suture.

In the *in-vitro* experiment, there are some differences between the extracted $\mu_s'(\lambda)$ of bone powder and intact bone, but during the process of bone growth of mid-palatal suture, the bone mostly grows in spiny, conical, and other small shapes, and the growth distribution is random. Therefore, compared to intact bone, the extracted $\mu_s'(\lambda)$ of the growing bone is expected to decrease, which may be represented by the optical properties of bone powders. the extracted $\mu_a(\lambda)$ of bone powder is $0.1\,\mathrm{cm}^{-1}$, which indicates that visible light absorption in bone powder had little influence compared with hemoglobin solution and the content of hemoglobin solution became the main factor in the extracted $\mu_a(\lambda)$. The measured hemoglobin concentration increased from 9.91 μM/ml to 44.39 μM/ml when the hemoglobin solution increased from 0.1800g to 0.7775g and the total amount of weight (bone powders and hemoglobin solution) was still the same. Similarly, when the hemoglobin solution dropped back to baseline, the measured hemoglobin concentration also dropped to the same value as that of baseline. The change of measured hemoglobin concentration also indicated that the detection ability of the DRS system can pass through the small-intestinal mucosa with a thickness of 1 mm, and the detection depth of the DRS system can be further increased by changing the probe geometry and the enhancement of source power.

According to the physical model in the experiment, DRS system can detect the content of hemoglobin, through mucosal tissue, in the uneven distribution of blood and bone paste. In human mid-palatal suture, the blood content may be used to quantify the size of suture gap and suture maturation. There are still many problems to be answered before DRS can be used for practical dental diagnosis and treatment. For example, multiple DRS measurements have to be made and the detection position should be consistent across samples, but it is difficult to do so in patients. During measurements, we also need to consider the influence of probe pressure because too much pressure may squeeze the blood in the capillary vessels out of the detection area, resulting in inaccurate measurement. Finally, the probe disinfection before human test also needs to be considered in follow-up work.

In general, this chapter investigated the potential of DRS in assessing human mid-palatal suture maturation after RPE. With the *in-vitro* experiment, we showed that the DRS system had the ability to detect submucosal hemoglobin concentration in the environment of cross distribution of blood and bone using a physical model.

Chapter 5 LIMITATIONS AND FUTURE WORK

The long-term goal of this study is to design a non-invasive device to assess the mid-palatal suture maturation after active RPE, which provides a reference to determine when to remove the RPE appliance for the follow-up orthodontic treatment. A robust DRS system for determining hemoglobin content and optical properties for mid palatal suture maturation is yet to be implemented in a clinical setting. The relationship between the size of suture gap and blood content has been studied using a simulated physical model. Some of the major limitation of this study and future directions are discussed below.

a) In *in-vivo* experiments, changes in the pressure between the probe tip and biological tissue may change the measured tissue values. Blood in human capillaries can spread around the pressure area after extrusion. The mid-palatal suture after RPE lacks the support of bone, and thus is soft and unstable. Changing pressure may have a greater impact on the measurements.

Yu et al. integrated a DFPI pressure sensor in the fiber optic probe to receive the interferogram of the sensor through the infrared band, and finally generate real-time pressure information [44]. The advantage of a pressure sensor is that it can measure the pressure information in real time without disturbing the light transmission of DRS system. In future work, the integrated pressure sensor may be used to monitor the pressure and to ensure the stability of the pressure for *in vivo* experiments.

b) Another major limitation of using DRS would be in the actual human detection process. Human oral cavity is limited, and patients need to wear expanders all the time after active RPE. The effective detection area of DRS system thus becomes very small. Currently, the designed fiber optical probe uses forward-firing fiber, which is not conducive to measurement in the narrow space of the mouth, and it may cause excessive bending or even breaking of the optical fibers. In contrast, side-firing fibers can bring more flexibility to the probe design and can take advantage of the gap between expander and oral mucosa for measurement.

c) The last issue is that after RPE, a wide suture gap may exceed the measurement range of the sampling area of the fiber optical probe. After active RPE treatment, the width of suture gap can reach 5mm or larger. However, due to the limitation of light penetration, the separation between illumination fiber and detection fiber should not be too large to ensure that the detection fiber can receive enough signals. Moreover, large suture gap will cause the blood content to surge, which will greatly reduce the optical signal, leading to inaccurate measurement.

References

1. McNamara JA. Maxillary transverse deficiency. Am J Orthod Dentofac Orthop. 2000;117:567–70.

2. Ekstrom C. Hericsson C, Jensen R. Mineralization in the midpalate suture after orthodontic expansion. Am J. Orthod Dentofaciqal Orthop 1977;2:449-55.

3. Hass AJ. Palatal expansion:just the beginning of Dentofacial orthodpedics. Am J. Orthod Dentofaciqal Orthop 1970;57:219-55.

4, Isiksal E, Hazar S, Akyalcin S. Smile esthetics: perception and comparison of treated and untreated smiles. Am J Orthod Dentofac Orthop. 2006;129:8–16

5. Bishara SE, Staley RN. Maxillary expansion: clinical implications. Am J Orthod Dentofac Orthop. 1987;91:3–14.

6. Lin L, Ahn HW, Kim SJ, Moon SC, Kim SH, Nelson G. Tooth-borne vs boneborne rapid maxillary expanders in late adolescence. Angle Orthod. 2015;85: 253–62.

7. Angelieri F, Cevidanes LH, Franchi L, Gonçalves JR, Benavides E, McNamara JA Jr. Midpalatal suture maturation: classification method for individual assessment before rapid maxillary expansion. Am J Orthod Dentofac Orthop. 2013;144:759–69.

8. Baccetti T, Franchi L, Cameron CG, McNamara JA Jr. Treatment timing for rapid maxillary expansion. Angle Orthod. 2001;71:343–50.

9. Sumer AP, Ozer M, Sumer M, Danaci M, Tokalak F, Telcioglu NT. Ultrasonography in the evaluation of midpalatal suture in surgically assisted

rapid maxillary expansion. J Craniofac Surg. 2012;23:1375–7.

10. Melsen B. Palatal growth studied on human autopsy material. A histologic microradiographic study. Am J Orthod. 1975;68:42–54.

11. Persson M, Thilander B. Palatal suture closure in man from 15 to 35 years of age. Am J Orthod. 1977;72:42–52.

12. Franchi L, Baccetti T, Lione R, Fanucci E, Cozza P. Modifications of midpalatal sutural density induced by rapid maxillary expansion: a low-dose computed-tomography evaluation. Am J Orthod Dentofac Orthop. 2010; 137:486–8. discussion 12A-13A

13. Korbmacher H, Schilling A, Püschel K, Amling M, Kahl-Nieke B. Agedependent three-dimensional microcomputed tomography analysis of the human midpalatal suture. J Orofac Orthop. 2007;68:364–76.

14. Maffulli N, Hughes T, Fixsen JA. Ultrasonographic monitoring of limb lengthening. *J Bone Joint Surg Br* 1992; 74: 130–2.

15. J. Q. Brown, K. Vishwanath, G. M. Palmer, and N. Ramanujam, Curr. Opin. Biotechnol. 20, 119 (2009).

16. B. Chance, "Near-infrared images using continuous, phase-modulated, and pulsed light with quantitation of blood and blood oxygenation", in Advances in Optical Biopsy and Optical Mammography, R. R. Alfano, Ed. (The New York Academy of Sciences, New York, New York, p. 29.

17. T. J. Flotte, Adv. Opt. Biopsy Opt. Mammogr., Annals NY Acad. Sci. 838, 143 (1998).

18. N. S. Nishioka, Can. J. Gastroent. 17, 376 (2003).

19. M. A. Suhr, C. Hopper, L. Jones, J. G. George, S. G. Bown, and A. J. MacRobert, Int. J. Oral Maxillofacial Surg. 29, 453 (2000).

20. K. Svanberg, C. Klinteberg, A. Nilsson, I. Wang, S. Andersson-Engels, and S. Svanberg, Adv. Opt. Biopsy Opt. Mammogr., Annals NY Acad. Sci. 838, 123 (1998).

21. T. Vo-Dinh, M. Panjehpour, and B. Overholt, ‘‘Laser-induced fluorescence for esophageal cancer and dysplasia diagnosis’’, in Advances in Optical Biopsy and Optical Mammography, R. R. Alfano, Ed. (The New York Academy of Sciences, New York, 1998), p. 116.

22. G. Zonios, R. Cothren, J. M. Crawford, M. Fitzmaurice, R. Manoharan, J. Van-Dam, and M. S. Feld, Adv. Opt. Biopsy Opt. Mammogr., Annals NY Acad. Sci. 838, 108 (1998).

23. M. Chandra, J. Scheiman, D. Heidt, D. Simeone, B. McKenna, and M. A. Mycek, J. Biomed. Opt. 12, 060501 (2007).

24. M. Chandra, K. Vishwanath, G. D. Fichter, E. Liao, S. J. Hollister, and M. A. Mycek, Opt. Exp. 14, 6157 (2006).

25. Sircan-Kucuksayan A, Uyuklu M, Canpolat M. Diffuse reflectance spectroscopy for the measurement of tissue oxygen saturation. Physiol Meas. 2015;36(12):2461-2469. doi:10.1088/0967-3334/36/12/2461.

26. A. N. Yaroslavsky, A. V. Priezzhev, J. Rodriguez, I. V. Yaroslavsky, and H. Battarbee, "Optics of Blood," in Handbook of Optical Biomedical Diagnostics, V. V.

Tuchin, ed. (SPIE - The International Society for Optical Engineering, Bellingham, 2002).

27. L. Wang, S. L. Jacques, and L. Zheng, "MCML--Monte Carlo modeling of light transport in multi-layered tissues," Comput Methods Programs Biomed 47, 131-146 (1995).

28. G. Zonios, L. T. Perelman, V. Backman, R. Manoharan, M. Fitzmaurice, J. Van-Dam, and M. S. Feld, "Diffuse reflectance spectroscopy of human adenomatous colon polyps in vivo," Appl. Opt. 38, 6628-6637 (1999).

29. J. C. Finlay and T. H. Foster, "Hemoglobin oxygen saturations in phantoms and *in vivo* from measurements of steady-state diffuse reflectance at a single, short source–detector separation," Med. Phys. 31, 1949–1959 (2004).

30. P. Thueler, I. Charvet, F. Bevilacqua, M. St. Ghislain, G. Ory, P. Marquet, P. Meda, B. Vermeulen, and C. Depeursinge, "*In-vivo* endoscopic tissue diagnostics based on spectroscopic absorption, scattering, and phase function properties," J. Biomed. Opt. 8, 495–503 (2003).

31. C. F. Bohren and D. R. Huffman, *Absorption and Scattering of Light by Small Particles* (Wiley, 1983).

32. Wang L, J.S., Zheng L, MCML--Monte Carlo modeling of light transport in multi-layered tissues. Computer methods and programs in biomedicine, 1995. 47(2): p. 131-146.

33. Palmer, G.M. and N. Ramanujam, Monte Carlo-based inverse model for calculating tissue optical properties. Part I: Theory and validation on synthetic phantoms. Appl Opt, 2006. 45(5): p. 1062-71.

34. Frei RW. Diffuse Reflectance Spectroscopy; Applications, Standards, and Calibration (With Special Reference to Chromatography). 1976;(August):551-565.

35. Wilson RH, Mycek M. Models of light propagation in human tissue applied to cancer diagnostics. Technol Cancer Res Treat. 2011;10(2):121-134. doi:10.7785/tcrt.2012.500187.

36. V. T. Chang, P. S. Cartwright, S. M. Bean, G. M. Palmer, R. C. Bentley, and N. Ramanujam, "Quantitative physiology of the precancerous cervix in vivo through optical spectroscopy," Neoplasia 11(4), 325–332 (2009).

37. Langhout GC, Spliethoff JW, Schmitz SJ, et al. Differentiation of healthy and malignant tissue in colon cancer patients using optical spectroscopy: A tool for image-guided surgery. Lasers Surg Med. 2015;47(7):559-565. doi:10.1002/lsm.22388.

38. Anand S, Sujatha N, Narayanamurthy VB, Seshadri V, Poddar R. Diffuse reflectance spectroscopy for monitoring diabetic foot ulcer - A pilot study. Opt Lasers Eng. 2014;53:1-5. doi:10.1016/j.optlaseng.2013.07.020.

39. Pike Technologies. Diffuse Reflectance – Theory and Applications.

40. Sircan-Kucuksayan A, Uyuklu M, Canpolat M. Diffuse reflectance spectroscopy for the measurement of tissue oxygen saturation. Physiol Meas. 2015;36(12):2461-2469. doi:10.1088/0967-3334/36/12/2461.

41. Vishwanath K, Chang K, Klein D, et al. Portable, fiber-based, diffuse reflection spectroscopy (DRS) systems for estimating tissue optical properties. Appl Spectrosc. 2011;65(2):206-215. doi:10.1366/10-06052.

42. Yu B, Shah A, Nagarajan VK, Ferris DG. Diffuse reflectance spectroscopy of epithelial tissue with a smart fiber-optic probe. Biomed Opt Express. 2014;5(3):675-689. doi:10.1364/BOE.5.000675.

43. Nagarajan, V.K. and B. Yu, Monitoring of tissue optical properties during thermal coagulation of ex vivo tissues. Lasers Surg Med, 2016. 48(7): p. 686-94.)

44. B. Yu, D. W. Kim, J. Deng, H. Xiao, and A. Wang, "Fiber Fabry-Perot sensors for detection of partial discharges
in power transformers," Appl. Opt. 42(16), 3241–3250 (2003).

45. Am J Orthod Dentofacial Orthop. Author manuscript; available in PMC 2014 Oct 5.Am J Orthod Dentofacial Orthop. 2013 Nov; 144(5): 759–769.
doi: 10.1016/j.ajodo.2013.04.022

46. Arifler, D., et al., Reflectance spectroscopy for diagnosis of epithelial precancer: model-based analysis of fiber-optic probe designs to resolve spectral information from epithelium and stroma. Appl Opt, 2005. 44(20): p. 4291-305.

47. Welch, A.J., & Gemert, M. J., Optical-Thermal Response of LaserIrradiated Tissue. 2011.

48. Wilson RH, Mycek M. Models of light propagation in human tissue applied to cancer diagnostics. Technol Cancer Res Treat. 2011;10(2):121-134.

49. Angell EC. Treatment of irregularity of the permanent or adult teeth. Dental Cosmos. 1860;1:540-44.

50. Anderson RR, Parrish JA. The optics of human skin. J Invest Dermatol. 1981; 77(1): 13-19. Doi:10.1016/j.artres.2008.11.002

51. Welch, A.J., & Gemert, M. J., Optical-Thermal Response of LaserIrradiated Tissue. 2011.

52. Elisabeth J. M. Baltussen, Petur Snæbjörnsson, "Diffuse reflectance spectroscopy as a tool for real-time tissue assessment during colorectal cancer surgery," J. Biomed. Opt. 22(10) 106014 (27 October 2017) https://doi.org/10.1117/1.JBO.22.10.106014

53. Cerussi A, Hsiang D, Shah N, et al. Predicting response to breast cancer neoadjuvant chemotherapy using diffuse optical spectroscopy. Proc Natl Acad Sci USA. 2007;104:4014–4019.

54. X. Hong, V. K. Nagarajan, D. H. Mugler, and B. Yu, “Smartphone microendoscopy for high resolution fluorescence imaging,” J. Innovative Opt. Health Sci., vol. 9, no. 5, 2016, Art. no. 1650046.

55. Roggan A, Friebel M, Do Rschel K, Hahn A, Mu Ller G. Optical Properties of Circulating Human Blood in the Wavelength Range 400-2500 nm. J Biomed Opt. 1999 Jan;4(1):36-46. doi: 10.1117/1.429919. PMID: 23015168.

56. Heesoo Oh, Joorok Park, Manuel O. Lagravere-Vich, Comparison of traditional RPE with two types of micro-implant assisted RPE: CBCT study, Seminars in Orthodontics,

Volume 25, Issue 1, 2019, Pages 60-68, ISSN 1073-8746,

https://doi.org/10.1053/j.sodo.2019.02.007.